Molecular Dynamics Modeling of Clay Minerals. 1. Gibbsite, Kaolinite, Pyrophyllite, and Beidellite

Brian J. Teppen,*,† Kjeld Rasmussen,‡ Paul M. Bertsch,† David M. Miller,§ and Lothar Schäfer||

Advanced Analytical Center for Environmental Sciences, Savannah River Ecology Laboratory, University of Georgia, P.O. Drawer E, Aiken, South Carolina 29802, Department of Chemistry, Building 207, The Technical University of Denmark, DK-2800 Lyngby, Denmark, Department of Agronomy, 115 Plant Science Building, University of Arkansas, Fayetteville, Arkansas 72701, and Department of Chemistry and Biochemistry, 115 Chemistry Building, University of Arkansas, Fayetteville, Arkansas 72701

Received: May 30, 1996; In Final Form: December 12, 1996[⊗]

A molecular dynamics model for clays and the oxide minerals is desirable for studying the kinetics and thermodynamics of adsorption processes. To this end, a valence force field for aluminous, dioctahedral clay minerals was developed. Novel aspects of this development include the bending potential for octahedral O−Al−O angles, which uses a quartic polynomial to create a double-well potential with minima at both 90° and 180°. Also, atomic point charges were derived from comparisons of ab initio molecular electrostatic potentials with X-ray diffraction-based deformation electron densities. Isothermal−isobaric molecular dynamics simulations of quartz, gibbsite, kaolinite, and pyrophyllite were used to refine the potential energy parameters. The resultant force field reproduced all the major structural parameters of these minerals to within 1% of their experimentally determined values. Transferability of the force field to simulations of adsorption onto clay mineral surfaces was tested through simulations of Na^+, Ca^{2+}, and hexadecyltrimethylammonium ($HDTMA^+$) in the interlayers of beidellite clays. The new force field worked rather well with independently derived nonbonded parameters for all three adsorbates, as indicated by comparisons between experimental and molecular-dynamics-predicted $d_{(001)}$ layer spacings of the homoionic beidellites.

Introduction

Data from experimental techniques that can probe clay minerals and their interfaces at the molecular scale, such as vibrational, NMR, neutron scattering, EXAFS, and XANES spectroscopies, and scanning probe microscopy are often difficult to interpret. Molecular dynamics simulations of clay minerals can potentially provide new constraints to aid those interpretations. Taken together, molecular-scale simulations and experimental investigations of clay−solution interfaces can further our understanding and control of chemical transport in the environment and help us to refine existing kinetic and thermodynamic models for sorption to soil colloids.

Until now, molecular simulations of clay interfaces have been limited to either static energy minimizations[1−4] or situations where the clay was fixed as a rigid lattice.[5−18] This approach has provided useful information about structures of solutions near the clay but has some inherent limitations. First, it is likely that motions of the clay surface atoms will influence the structure of the nearest water layers and the properties of solvated molecules and ions. For example, simulated diffusion rates within zeolite channels[19,20] can be much too rapid if the zeolite cage is held rigid. Second, dynamic modeling of sorption kinetics is necessary because activation energies for interfacial processes may be strongly dependent on surface phonons of the adsorbent.[21] Also, neutron diffraction and EXAFS provide averaged interatomic distances which are not modeled realistically if the simulated system is not dynamic. Finally, only a dynamic model for clays will allow the temperature dependence of mineral structures and spectra to be simulated.

The key factor precluding dynamic simulations of clay minerals has been a lack of an effective treatment for modeling the octahedral sheet. Indeed, the difficulty with octahedral coordination is one of the chief factors limiting the extension of molecular mechanics methods to inorganic systems.[22] In neutral dioctahedral phyllosilicate clays such as kaolinite and pyrophyllite, aluminum atoms are octahedrally coordinated by oxygen. This results in O−Al−O angles near both 90°and 180°, which are not easily modeled by conventional molecular mechanics methods for organic compounds.

In their SHAPES force field,[23] Landis' group proposed using a cosine function for angle bending,

$$V = k_\theta[1 + \cos(n\theta + \varphi)] \qquad (1)$$

where V is the potential energy of bending, k_θ is the angular force constant, n is the periodicity of the angle θ, and φ is the phase shift of the potential. This function works for octahedra if $n = 4$ and $\varphi = 180°$, because the function has minima at both 90° and 180°. Unfortunately, there is also a minimum at 0°, which can cause problems. The "universal force field," of Goddard's group[24] generalizes this Fourier-type angle-bending potential, along with some highly approximate rules for its application to the whole periodic table. None of these force fields has been carefully parameterized for aluminosilicates. Engelsen[25] proposed using only the repulsive part of the harmonic angle-bending potential and showed that this was effective for octahedral systems, but then the lone pairs of all tetrahedral atoms such as oxygen must be included or else all angles with oxygen at the apex will tend toward 180°.

In this paper, we present a new approach for performing molecular dynamics simulations of phyllosilicate clays and other

* Author to whom correspondence should be addressed. Phone: 803-725-8157, FAX: 803-725-3309, E-mail: teppen@srel.edu.
† University of Georgia.
‡ The Technical University of Denmark.
§ Department of Agronomy, University of Arkansas.
|| Department of Chemistry and Biochemistry, University of Arkansas.
⊗ Abstract published in *Advance ACS Abstracts,* February 15, 1997.

S1089-5647(96)01577-5 CCC: $14.00

octahedral systems. Our general strategy has been to modify commercially available software[26,27] that already contains an effective valence force field for tetrahedral aluminosilicates.[28,29] Using the valence force constants from the previous force field[28,29] as far as possible, new nonbonded terms were refined with improved electrostatic charges by modeling the crystal structures of some representative clay minerals. The resulting parameter set is applicable to the study of clay interfacial adsorption processes.

Methods

(a) General Considerations. It is generally accepted that Si−O bonding is predominantly covalent[30] but octahedral Al−O bonding is considered mostly ionic.[31,32] Even aluminum oxides, however, are somewhat covalent, as evidenced by electron density bridges along Al−O bonds.[31,32] We chose to develop covalent-type potentials for all the clay mineral atoms, in order to facilitate the future modeling of the minerals with covalently bonded species such as water and organic solutes. Also, ionic models with shell polarization terms are of limited use for molecular dynamics because of the large force constant[33,34] linking oxygen cores with their polarization shells. Extremely small time steps would be required to avoid excessive distortion of these shells.

Hill and Sauer[28,29] used quantum chemical results as a basis to derive parameters for modeling quartz and siliceous zeolites, as well as sites of aluminum substitution in zeolite frameworks. They used the robust functional form of the valence force field cff91[35] because their ab initio database was large enough to fit the many parameters required, including anharmonicities and parameter-coupling cross terms. These cross terms enable explicit modeling of linkages such as exist between Si−O stretching and Si−O−Si bending potentials.[36−38] We built upon the zeolite parameters[29] to create a cff91 force field (Table 1) for dynamic modeling of clay minerals.

(b) Definition of the Angle-Bending Potential. The cff91 force field[35] treats the angle-bending potential as a function of the form

$$V = k_4(\theta - \theta_o)^4 + k_3(\theta - \theta_o)^3 + k_2(\theta - \theta_o)^2 \qquad (2)$$

The inclusion of cubic and quartic terms is normally used to create anharmonicity in the otherwise quadratic angle deformation potential. The potential can also yield a multiminimum potential when the parameters are chosen judiciously. For example, given an arbitrary force constant $A > 0$, if one sets $\theta_o = 135°$, $k_4 = A$ kcal mol^{-1} rad^{-4}, $k_3 = 0$ kcal mol^{-1} rad^{-3} and $k_2 = -1.234A$ kcal mol^{-1} rad^{-2}, then eq 2 yields a function with dual minima at 90° and 180° (Figure 1).

Differentiating eq 2 twice and substituting $k_4 = -k_2/1.234$ yields

$$\frac{\partial^2 V}{\partial \theta^2}\Big|_{\theta = 90° \text{ or } 180°} = -4k_2 \quad \Rightarrow \quad \tilde{\nu} = \frac{108.59}{r_{\mathrm{Al-O}}}\sqrt{-\frac{4k_2}{\mu}} \qquad (3)$$

where μ is the reduced mass (in amu) of the O−Al−O bending vibration, the units of k_2 are kcal mol^{-1} rad^{-2}, and those of $\tilde{\nu}$ are cm^{-1}. Since the Al−O bond length is typically near 1.92 Å[32,39−41] and μ is roughly 4 amu,

$$\tilde{\nu} \approx 57\sqrt{-k_2} \qquad (4)$$

Estimates for the appropriate force constants were derived from two isomers of $Al(OH)_3(H_2O)_3$, which were optimized using HF ab initio calculations[42,43] with the MC6-311G** basis set.[44−47] Analytical force constants and harmonic vibrational frequencies were computed and scaled[48] by 0.89.[49] Scaled frequencies of the HO−Al−OH angle bending modes in meridional and facial $Al(OH)_3(H_2O)_3$ averaged about 275 cm^{-1}, which implies values for k_2 near −23.4 kcal mol^{-1} rad^{-2} and k_4 of 19.0 kcal mol^{-1} rad^{-4}. These estimates were used as starting values and modified in the ensuing parameter refinement.

(c) Further Development of the Force Field. In order to adapt the cff91 force field to simulations of clay minerals, several new atom types had to be defined for the octahedral sheet (Table 1). Hill and Sauer's force constants[29] were used for the bond stretching and angle bending (excluding ocl-ao-ocl, vide supra) terms, but they were coupled with new equilibrium parameters.

All Al, O, and H torsional terms for sequences where octahedral Al was a terminal atom were again adapted directly from Hill and Sauer.[28,29] This was done by setting ao terms equivalent to their az atom type, ocl equivalent to their ob, and hcl equivalent to their hb. In the case of torsions where octahedral Al was one of the central atoms, all torsions were set to zero. This was done because the cff91 force field allows at most 3-fold torsional periodicity, but 4-fold periodicity is needed at octahedral centers.

(d) Non-bonded Parameters for Simulations of Aluminosilicate Surfaces. Hill and Sauer's force field[28,29] is based on Hartree−Fock calculations, which do not include electron correlation effects. Accounting for correlation, by fitting the force field to empirical data and/or to higher-quality calculations, is vitally important to parameter development.[50,51] Since electron correlation is the physical phenomenon that gives rise to dispersion forces, the force field from Hill and Sauer includes no dispersive terms. Also, Hill and Sauer used atomic charges which were derived from Hartree-Fock population analyses and were then, in an ad hoc way, cut in half. Since a primary goal of our modeling effort is to investigate interactions between minerals and physically adsorbed molecules and ions, we made an effort to improve these nonbonded potentials by adding dispersive forces and employing more realistic atomic charges.

We used the CHELPG method[52−54] to derive partial atomic charges from the MP2-optimized geometries of several small aluminosilicate molecules.[55] In addition, we also considered deformation electron densities derived from X-ray diffraction data of oxide crystals.[56] The latter are uncertain in many respects[30,57] but provide some physical basis for comparison with purely theoretical values derived from molecular electrostatic potentials. Deformation-density estimates for the charge on Si in silicates range from 0.85 to 2.56 elementary charge.[56] Our best estimate from molecular electrostatic potentials[55] is 1.4, near the center of this range. Simple electronegativity differences indicate that the Si−O bond is about 45% ionic, which implies a charge on Si of 1.80,[30] although Pauling[58] argued that pπ−dπ resonance should reduce this value to 1.0. Note that all of the theoretical and experimental estimates are far larger than the Si partial charge of 0.524 used by Hill and Sauer[28,29] in their silicate force field. We assigned charges of 1.4 to Si and −0.70 to each oxygen bridging two silicon atoms (Table 1); these charges were roughly three times larger than those employed in Hill and Sauer's model.

The choice of partial atomic charges is of considerable concern, since the mineral force field must be consistent with other force fields derived independently for water and solutes. The relative interaction energies for cations interacting with both water and a clay surface depend strongly on the charges assigned to oxygen in water and the mineral. In the case of typical water

TABLE 1: Force Field Parameters for Molecular Dynamics Simulations of Clay Minerals[a]

Atom Type Descriptions

ao	Al in octahedral coordination
ocl	O in the octahedral sheet, triply coordinated
hcl	H in clay mineral hydroxyl groups
sz	Si in tetrahedral coordination
az	Al in tetrahedral coordination
oss	O in Si−O−Si linkages
oas	O in Si−O-Al linkages in the tetrahedral sheet

Bond Stretching: $E_{IJ} = k2(r - r_0)^2 + k3(r - r_0)^3 + k4(r - r_0)^4$

I	J	r_0 (Å)	k_2 (kcal/(mol Å^2))	k_3 (kcal/(mol Å^3))	k_4(kcal/(mol Å^4))
sz	ocl	1.620	494.1	−36.7	2150.7
az	oas	1.780	328.7	−341.0	2189.0
az	ocl	1.780	328.7	−341.0	2189.0
ocl	hcl	0.988	656.8	−1627.5	3684.2
sz	oss	1.626	459.1	−672.4	443.4
ao	ocl	1.955	328.7	−341.0	2189.0

Angle bending: $E_{IJK} = k2(\theta - \theta_0)^2 + k3(\theta - \theta_0)^3 + k4(\theta - \theta_0)^4$

I	J	K	θ_o (deg)	k_2 (kcal/(mol rad^2))	k_3 (kcal/(mol rad^3))	k_4 (kcal/(mol rad^4))
ao	ocl	ao	109.5	195.3	48.9	185.3
ocl	ao	ocl	135.0	−40.0	0.0	32.4
ao	ocl	hcl	118.0	44.0	−53.4	103.4
sz	ocl	ao	124.5	195.3	48.9	185.3
az	ocl	ao	124.5	195.3	48.9	185.3
oss	sz	ocl	110.6	88.1	−57.0	92.5
oas	sz	ocl	110.6	88.1	−57.0	92.5
oas	az	ocl	104.5	300.1	−32.6	67.3

Torsional: $E_{IJKL} = \sum_{n=1}^{3} V_n[1 + \cos(n\phi - \phi_{0n})]$

I	J	K	L	V_1 (kcal/mol)	ϕ_{01} (deg)	V_2 (kcal/mol)	ϕ_{02} (deg)	V_3 (kcal/mol)	ϕ_{03} (deg)
ocl	ao	ocl	ao	0.00	0.0	0.00	0.0	0.00	0.0
ocl	ao	ocl	hcl	0.00	0.0	0.00	0.0	0.00	0.0
ocl	ao	ocl	sz	0.00	0.0	0.00	0.0	0.00	0.0
ocl	ao	ocl	az	0.00	0.0	0.00	0.0	0.00	0.0
oas	az	ocl	ao	−4.11	0.0	3.59	0.0	0.26	0.0
oss	sz	ocl	ao	0.16	0.0	1.79	0.0	0.20	0.0
oas	sz	ocl	ao	−1.83	0.0	2.23	0.0	0.23	0.0

Nonbonded (1,2- and 1,3-Interactions Excluded): $E_{ij} = \sum_{i \neq j} \frac{A_i A_j}{r_{ij}^9} - \frac{B_i B_j}{r_{ij}^6} + \frac{332.07 q_i q_j}{r_{ij}}$

I	A_i (((kcal/mol) Å^9)$^{1/2}$)	B_i (((kcal/mol) Å^6)$^{1/2}$)	q_i (elementary charge)
sz	775	0.01	1.40
ocl	790	190	−0.91 to −1.11[b]
az	775	0.01	1.20
ao	2800	0.01	1.68
oas	635	140	−0.90
oss	635	140	−0.70
hcl	2.0	0.40	0.40

[a] Parameters were developed as described in the text. Force constants from the work of Hill and Sauer[29] on tetrahedral aluminosilicates were retained whenever possible. [b] Charge on ocl varied in order to maintain proper charge on the clay as a whole. Thus, when ocl was coordinated by Si and two octahedral Al, its charge was −0.91. When coordinated by tetrahedral Al and two octahedral Al, its charge was −1.11. When coordinated by H and two octahedral Al, its charge was −0.96.

models,[59,60] oxygen is assigned a charge near −0.8, which is comparable to our values for aluminosilicate oxygens, but by a factor of ∼3 more negative than those of Hill and Sauer. Thus, all else being equal, the force field of Hill and Sauer would be expected to predict outer-sphere complexation much more often than would the force field presented here.

When Al replaces Si in tetrahedral coordination, a structural negative charge is created in the mineral. Hill and Sauer[29] modeled systems where Al substitution was always accompanied by proton adsorption to neutralize this structural charge. In their model, substitution of Al for Si in a tetrahedral structure (without simultaneous adsorption of a proton) would result in a charge of 0.678 assigned to the aluminum, which is larger than the 0.524 charge on silicon. It does not seem realistic that the charge on the tetrahedral center would become more positive as a result of a substitution that gives rise to a net negative charge in the structure. In simulating clay minerals, we must be able to balance the structural negative charge created by substitution with positive counterions that are not part of the crystal structure, so a new method for modeling substitution sites is clearly needed. On the basis of MP2 ab initio calculations, the charge on Al computed from molecular electrostatic potentials is roughly 1.20, while the charge on the neighboring O is about −0.90, resulting in a net charge of −1.0

TABLE 2: Nonbonded Parameters for Modeling the Interactions of Beidellite Clay Minerals with Na^+, Ca^{2+}, and $HDTMA^+$ [a]

Nonbonded (1,2- and 1,3-interactions excluded): $E_{ij} = \sum_{i \neq j} \frac{A_i A_j}{r_{ij}^9} - \frac{B_i B_j}{r_{ij}^6} + \frac{332.07 q_i q_j}{r_{ij}}$

atom type	description	A_i (((kcal/mol) Å^9)$^{1/2}$)	B_i (((kcal/mol) Å^6)$^{1/2}$)	(elementary charge)
Na	Na^+ ion	79.0	3.89	1.000
cal	Ca^{2+} ion	162	18.82	2.000
n4	N atom in an ammonium group	73.7	15.3	−0.628
c3	methyl C	170.2	26.0	−0.159[b]
c2	methylene C	170.2	26.0	−0.106[c]
hc	H atom in saturated hydrocarbons	27.8	6.58	0.053

[a] For the simulations reported in this study, all internal degrees of freedom for $HDTMA^+$ were allowed to vary. Only the nonbonded terms are tabulated since they govern interactions with the clay. [b] Charge is +0.248 if bonded to ammonium N. [c] Charge is +0.301 if bonded to ammonium N.

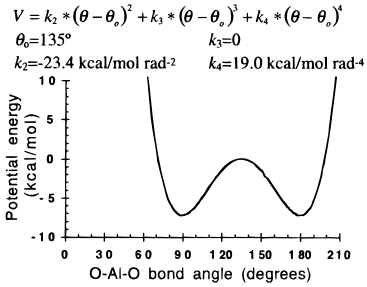

Figure 1. Octahedral O−Al−O angle-bending potential that allows multiple equivalent minima through specification of a single "equilibrium" angle.

on the Al tetrahedron compared to the Si tetrahedron (a manuscript on the ab initio results is in preparation). This smearing of the negative charge due to isomorphic substitution over the entire tetrahedron seems more physically reasonable[61] than simply decreasing the charge on Al by 1 elementary charge compared to Si, as is often done for clays.[5−13]

When Al is octahedrally coordinated by O, the CHELPG method[52−54] yields charges on Al that vary from 1.5 to 2.0. Deformation electron densities based on X-ray diffraction of diaspore AlOOH,[32] corundum Al_2O_3,[62] the clinopyroxene $LiAlSi_2O_6$[63], and euclase $AlBeSiO_4(OH)$[64] yield estimates of 1.47 ± 0.26, 1.32 ± 0.05, 2.4, and 1.8 ± 0.1, respectively, for octahedrally coordinated Al. Electronegativity differences indicate that the Al−O bond is about 56% ionic, which implies a charge on Al near 1.68. Since charges obtained by all these methods were in the same range, we chose 1.68 for the charge on Al when coordinated by six oxygens.

(e) Clay Mineral Simulations. To develop and test the efficacy of the force field, clay minerals with strictly Al in the octahedral sheet and either Al or Si in the tetrahedral sheet were constructed and simulated. The framework of kaolinite (half unit cell composition $Al_2Si_2O_5(OH)_4$) was constructed using the structure refined by Bish[41] from the neutron diffraction data of Young and Hewat[65] collected at 1.5 K. Coordinates for the dioctahedral, unsubstituted clay mineral pyrophyllite (half unit cell composition $Al_2Si_4O_{10}(OH)_2$) were taken from Lee and Guggenheim's refinement of X-ray data collected at room temperature.[40]

Two unit cells of this pyrophyllite were fused and two tetrahedrally coordinated Si atoms substituted by Al to produce an $Al_8(Al_2Si_{14})O_{40}(OH)_8$ supercell of idealized beidellite. This model mineral had a cation exchange capacity (CEC) of 135 cmol kg^{-1}. In each supercell, one substitution site was randomly located in each tetrahedral sheet and the negative charge was neutralized by either two Na^+ or one Ca^{2+}. In addition, two reduced-charge beidellites were created for simulations of different $CH_3(CH_2)_{15}N(CH_3)_3^+$ ($HDTMA^+$) surface coverages. To do so, a supercell of six unit cells was created and aluminum was substituted for silicon in either two (resultant CEC: 45 cmol kg^{-1}) or four (resultant CEC: 90 cmol kg^{-1}) tetrahedral sites per supercell.

Constructing supercells in this manner creates highly ordered structures which do not truly represent the disordered systems found in nature. Investigation of the effects of different isomorphic substitution patterns through simulations of larger supercells is an important task that remains for future studies.

In the ensuing refinement of parameters the repulsive and dispersive van der Waals parameters were adjusted until they best reproduced the crystal structures of pyrophyllite,[40] kaolinite,[41] and gibbsite[39]. The $d_{(001)}$ layer repeat distances of these lamellar minerals are extremely sensitive to the nonbonded parameters of the force field and they form a complementary set, since they represent interactions of two tetrahedral sheets, one tetrahedral and one octahedral sheet, and two octahedral sheets, respectively. The crystal structure of quartz[66,67] was also used to constrain parameters.

The nonbonded potentials for tetrahedral Si and octahedral Al resulting from this work feature very large repulsive terms (Table 1). It was not possible to reproduce both the $d_{(001)}$ spacings and the intralamellar structures with van der Waals atom "sizes" that correspond to ionic radii.[68−70] This is due to the implementation[27] of the cff91 force field, which does not include 1,3-nonbonded Coulombic and van der Waals terms because all 1,3-interactions are included in the angle bending terms. Thus, the shortest nonbonded interactions that are considered (i.e., 1,4-interactions), always involve two atoms of opposite charge and are dominated by attractive Coulomb forces. This necessitates strongly repulsive 1,4-van der Waals terms to keep the mineral structures from collapsing.

Force field parameters for all adsorbates were derived independently of the clay force field. New nonbonded parameters for Na^+ and Ca^{2+} were developed for the Lennard-Jones 9−6 functional form of the cff91 force field, and the nonbonded terms are compiled in Table 2. Briefly, the required Lennard-Jones 9−6 parameters were found by setting the dispersive terms (B_i) equal to those of Åqvist[71] and then varying the repulsive terms (A_i) until the minima in the resultant metal−oxygen potential energy plots matched those of Åquist (Figure 2). Parameters for $HDTMA^+$ were taken from the Biosym database[26,27] (Table 2). The current study provides an opportunity to examine whether the independently derived parameters for metals and organics will work together with those of the clay force field to make reasonable predictions for the $d_{(001)}$ repeat distances of beidellites.

All simulations reported here employed three-dimensionally periodic boundary conditions[72] and imposed no space group symmetry other than *P*1. All simulations were performed in the isothermal−isobaric ensemble[73] using the Discover module of the Biosym molecular modeling suite[26] with the pressure set

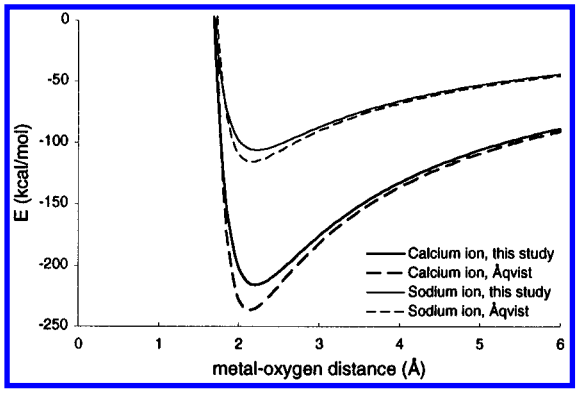

Figure 2. Metal−oxygen nonbonded potentials for aqueous Na^+ and Ca^{2+}, compared with those of Åqvist (ref 71). The present study required potentials in the Lennard-Jones 9−6 form, whereas Åqvist's potentials were of the 12−6 form.

to 100 kPa, the temperature to 298 K, and a timestep of 0.5 fs. The temperature was controlled by direct velocity scaling and our ensemble averages were typically 298 ± 5 K. The pressure was controlled by the Parrinello−Rahman method.[27] Instantaneous pressures varied considerably during our simulations but maintained a constant mean that was 0 ± 2 GPa.

We used Karasawa and Goddard's[74] Ewald-inspired lattice sums, as implemented in the Discover code, for calculating both the Coulombic and dispersive contributions to the energies and forces. In this scheme, the Ewald parameter is automatically chosen (based on unit cell dimensions) and an energy accuracy parameter is specified (here, 0.0025 kcal mol^{-1}). These two values were used to calculate the real-space and reciprocal-space cutoffs necessary to achieve the given accuracy.[74] Short-range van der Waals repulsion energies were computed in the all-image convention, again using the accuracy parameter to determine unit-cell-dependent cutoff radii.[74] Tests of this overall method show that nonbonded energies were accurate to within 0.005% of their asymptotic values.

Results and Discussion

(a) Molecular Dynamics Simulations of Gibbsite, Kaolinite, and Pyrophyllite. Randomly chosen snapshots from molecular dynamics simulations of gibbsite, kaolinite, and pyrophyllite are shown for comparison with the experimental structures (Figure 3). These are the first molecular dynamics simulations reported for any of these minerals, and some aspects of these comparisons are quantified in Table 3. Oscillations in the $d_{(001)}$ spacings of the clays generally attained equilibrium within a few ps, whereas 5−20 ps were required to stabilize the potential energy (Figure 4). Therefore, at least 50 ps of molecular dynamics were always used to gather the data in Table 3.

The gibbsite structure was reproduced adequately. The *b* axis was too large by 1%, but the simulated *a* axis length and the

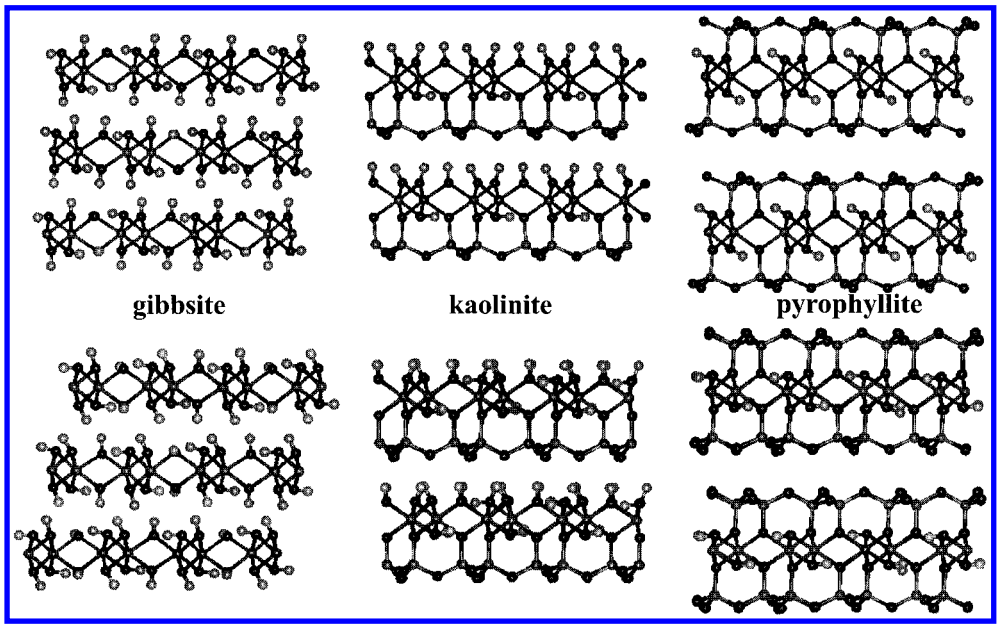

Figure 3. Comparisons of experimentally determined crystal structures (top) with typical snapshots from molecular dynamics simulations (bottom).

TABLE 3: Molecular Dynamics Structures of Layered Minerals Compared with Crystal Structure Refinements for Pyrophyllite, Kaolinite, and Gibbsite. All distances in Å

	pyrophyllite		kaolinite		gibbsite	
mineral parameter	model	exptl[a]	model	exptl[b]	model	exptl[c]
a axis length	5.18 ± 0.02	5.160	5.14 ± 0.02	5.154	5.08 ± 0.02	5.078
b axis length	9.02 ± 0.07	8.966	8.93 ± 0.03	8.942	8.77 ± 0.02	8.684
layer ***d*** spacing[d]	9.31 ± 0.04	9.190	7.10 ± 0.02	7.131	9.70 ± 0.03	9.706
density (g cm^{-3})	2.75 ± 0.02	2.815	2.62 ± 0.01	2.608	2.40 ± 0.01	2.421
Al−O bond length	1.92 ± 0.03	1.911	1.92 ± 0.03	1.907	1.90 ± 0.03	1.903
Si−O bond length	1.63 ± 0.03	1.618	1.63 ± 0.03	1.614		
O−H bond length	0.97 ± 0.02	0.970[e]	0.97 ± 0.02	0.977	0.97 ± 0.01	0.864[e]

[a] Reference 40. [b] Reference 41. [c] Reference 39. [d] Defined as the crystallographic repeat distance normal to the ***ab*** plane. This value is reported in lieu of the ***c*** axis length because relative translations of adjacent layers during molecular dynamics often resulted in large, distorted values for ***c***, even though the ***d***-spacing remained nearly constant. This was especially common for pyrophyllite. [e] These were X-ray diffraction studies, so the O−H bond length was estimated for pyrophyllite and the measurement for gibbsite would be expected to be too small. The kaolinite value was measured by neutron diffraction.

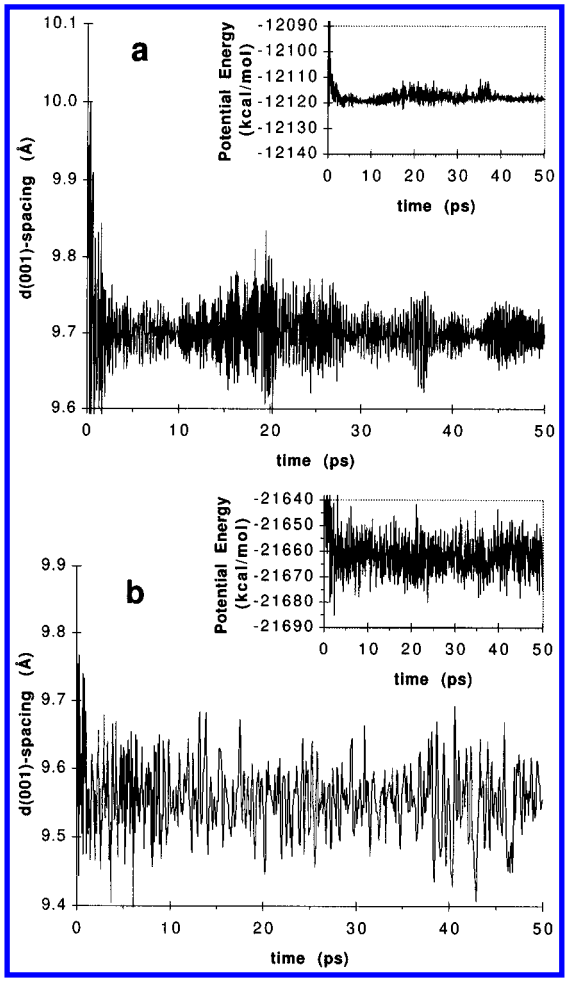

Figure 4. Evolution of the $d_{(001)}$ spacing and total potential energy during isothermal−isobaric molecular dynamics simulations of clay minerals. The examples shown are (a) gibbsite and (b) Ca-beidellite.

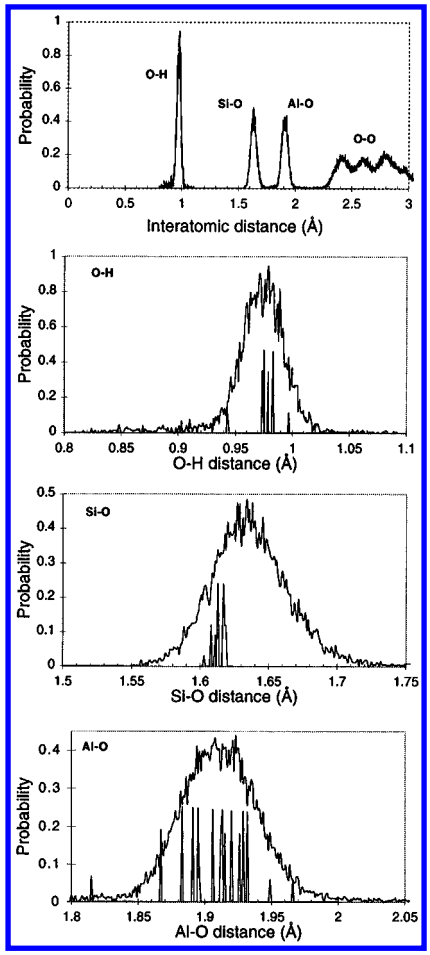

Figure 5. The simulated total radial distibution function for kaolinite at 298 K (top) and expanded views of the O−H, Si−O, and Al−O bonding regions. In the total radial distribution, contributions from interlayer O···O and O···H nonbonded interactions have been omitted. In the expanded views, the spikes indicate distances determined by neutron diffraction at 1.5 K.[41]

$d_{(001)}$ spacing were accurate. The hydrogen-bonding pattern between the layers changed somewhat (Figure 3), causing a slight relative translation (parallel to the (001) plane) of the layers compared with their experimental positions.[39] The hydroxyl groups typically remained near their experimental orientations, but the layer translation allowed about twice as many (but longer and weaker) interlayer hydrogen bonds to form as observed experimentally. This relative translation of neighboring gibbsite layers also changed the distribution of interlayer O···O nonbonded distances somewhat. In the experimental structure,[39] the nearest O···O nonbonded interlayer contacts average 2.84 Å (between H-bond donors and acceptors) and the next-nearest interlayer O···O distances are 3.7 Å or longer. In our simulations, the interlayer O···O distances were rarely as short as 2.8 Å, but there were many more interlayer O···O distances in the 3.0−3.3 Å range. The interlayer spacing, determined by a balance between O···O nonbonded repulsions and H-bonding attractions, agreed very well with the experimental value.

Some changes in interlayer hydrogen bonding were also evident in the molecular dynamics of kaolinite. The experimental crystal structure[41] indicates that all three of the crystallographically unique interlayer hydroxyls are involved in hydrogen bonds to the neighboring kaolinite layer. In the simulated structure, one of the three hydroxyls often adopts an orientation roughly parallel to the basal (001) plane, although it sometimes participates in interlayer hydrogen bonding. Note that this same hydroxyl is experimentally observed to be parallel to (001) in both gibbsite and pyrophyllite. Also, purely electrostatic calculations by Giese and Datta[75] predicted that the orientation of this hydroxyl would be roughly parallel to (001) in kaolinite. We have not yet discovered a set of parameters that would satisfy all three experimental structures for every proton (Figure 3).

The simulated *a* and *b* axis lengths for kaolinite were close to those observed experimentally. The simulated $d_{(001)}$ spacing of 7.10 Å is slightly smaller than the experimental value[41] (Table 3). The neutron diffraction data for kaolinite[41] allow a further test of the forcefield by comparing the computed radial distribution functions with experimentally determined distances (Figure 5). The locations of the O−H and Al−O peaks agree very well with the neutron diffraction data, but the Si−O peak is centered about 0.02 Å too long. The simulated unit cell for quartz with the present force field is $a = b = 4.92 \pm 0.02$ Å, $c = 5.43 \pm 0.02$ Å, $\alpha = \gamma = 90.0°$, and $\beta = 120.0°$, yielding a density of 2.63 ± 0.01 mg m^{-3}, and the Si−O, O···O, and Si···Si distributions are in good agreement with room-temperature neutron diffraction data.[67] In particular, the quartz Si−O bond seems to be modeled fairly well at 1.61 ± 0.03 Å, and it is unclear why this bond is slightly too long in kaolinite and pyrophyllite. In kaolinite, the three O···O peaks in Figure 5 correspond to shared edges of octahedra (∼2.4 Å), corners of tetrahedra (∼2.6 Å), and unshared edges of octahedra (∼2.8 Å), in good agreement with distributions found experimentally for clays.[40,41]

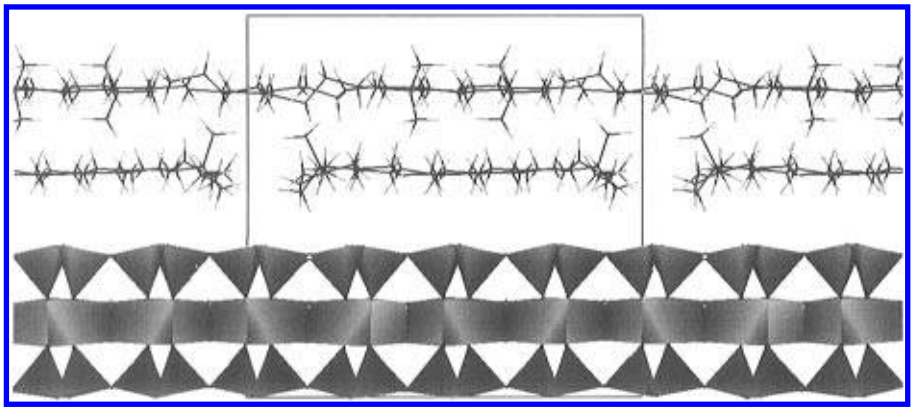

Figure 6. Representative snapshot of HDTMA-beidellite after isothermal−isobaric molecular dynamics equilibration. The central supercell, outlined in gray, contains four HDTMA and $Al_{24}(Al_4Si_{44})O_{120}(OH)_{24}$.

The structure of pyrophyllite was refined from X-ray data,[40] so the positions of hydrogen atoms were just estimated. These positions are the only major discrepancy between the experimental and simulated structures (Figure 3) and it is reasonable to believe that their orientations would match those determined by neutron diffraction for the inner hydroxyl of kaolinite.[41] The *a* and *b* axes for pyrophyllite were found to be slightly too large, perhaps indicating that nonbonded interactions between the octahedral and tetrahedral sheets may be excessive. The modeled $d_{(001)}$ spacing of pyrophyllite is also 1% too large, which might imply that the repulsive van der Waals parameter for oss should be decreased. This could not be done, however, without impairing the quality of the kaolinite model.

The translational shift of neighboring layers along the basal planes is an imperfection of the current procedure which is not expected to be an impediment to modeling clay−adsorbate interactions. Such shifts seem to be artifacts of molecular dynamics that arise when the initial velocities have a net shearing effect for which the restoring forces are small. Thus, the effect is most pronounced in pyrophyllite, whose interlayers are not stabilized by hydrogen bonding. The presence of interlayer adsorbates retards these shearing translations, and interlayer hydrogen bonding as in kaolinite or gibbsite precludes any large translational shifts. To correct the small shifts due to rearrangement of hydrogen-bonding patterns, improvements in nonbonded parameters are currently being explored using high-quality ab initio structures of suitable model compounds.

(b) Molecular Dynamics Simulations of Beidellites. Our chief interest in developing a valence force field for clays is to enable dynamic molecular modeling of adsorption and desorption processes. To test whether the current force field can be successfully employed in conjunction with parameters independently derived for other moieties, molecular dynamics simulations of Na-, Ca-, and HDTMA-beidellites were performed.

For Na^+ sorbed in the interlayer of a simulated high-charge (CEC = 135 cmol kg^{-1}) beidellite, isothermal−isobaric molecular dynamics resulted in an equilibrium clay $d_{(001)}$ spacing of 9.65 ± 0.03 Å. This value compares favorably with the experimental literature, which reports $d_{(001)}$ spacings for dry Na-smectites and Na-vermiculites between 9.5 and 10.0 A.[76−80] Also, the $d_{(001)}$ spacings of Na-beidellites tend to be 0.1−0.2 Å smaller than those of other Na-smectites[81] because most of their structural charge resides in the tetrahedral sheet, causing stronger average interlayer electrostatic forces.

For Ca^{2+} in the interlayer of a dry, high-charge beidellite, the simulated $d_{(001)}$ spacing was 9.54 ± 0.05 Å. Again, this agrees well with experiment, since Ca-beidellite $d_{(001)}$ spacings are observed to be slightly smaller than those for Na-beidellites under similar conditions.[81,82]

All Na^+ and Ca^{2+} cations nestled into siloxane ditrigonal cavities of opposing basal surfaces on the dry clay, thus bridging the interlayer region. The resultant unit-cell dimensions for the beidellites were 5.24 ± 0.02 and 8.95 ± 0.03 Å for the *a* and *b* axes, respectively.

Interlayer $HDTMA^+$ sufficient to neutralize the structural charge of a low-charge, hypothetical beidellite (CEC = 45 cmol kg^{-1}) resulted in a monolayer of $HDTMA^+$ between each clay layer. The $d_{(001)}$ spacing of this system, computed using isothermal−isobaric molecular dynamics, was 13.3 ± 0.1 Å. The experimentally observed $d_{(001)}$ spacing for similar quaternary amines is 13.6 ± 0.2 Å,[83−88] although 13.2 Å has been reported for a reduced-charge octadecylammonium-hectorite.[89] Lagaly[83] speculated that the low end of this range (i.e., ≤13.4 Å) corresponds to adsorbate conformations in which the planes of all C−C−C angles in the hydrocarbon tail are parallel to the clay basal plane. This was indeed the conformation adopted by $HDTMA^+$ during the course of our molecular dynamics simulations, even though the simulations began with half the C−C−C angles perpendicular to the basal plane.

When a model for medium-charge beidellite (CEC = 90 cmol kg^{-1}) was created and neutralized with $HDTMA^+$, an interlayer bilayer of the cation resulted. The $d_{(001)}$ spacing of this system after molecular dynamics equilibration was 17.3 ± 0.1 Å, compared with experimentally determined values in the range 17.8 ± 0.3 Å.[83−88] The clay−$HDTMA^+$ attractive forces might be too large in the model, or the simulated $d_{(001)}$ spacing may be smaller than experimental values because the model system is more regular than any real system. For example, all C−C−C angles of all HDTMA cations were approximately parallel to the basal plane at equilibrium in the simulations (Figure 6). Thus, the simulation may simply represent the absolute minimum $d_{(001)}$ spacing that could be observed for a bilayer of $HDTMA^+$.

Continuing parameter refinements are aimed at molecular dynamics simulations of hydrated clays. These calculations are highly sensitive to the water model employed because they must simultaneously reproduce the properties of bulk water (e.g., radial distribution and density) and those of water interacting with clays (e.g., hydration energies and $d_{(001)}$ layer spacings). For example, when the water model included with the Biosym database[26] was used with our clay parameters, Na- or Ca-smectites equilibrated in 50 ps unconstrained dynamics simulations with gravimetric water contents near 0.15 and 0.3 g/g yielded $d_{(001)}$ spacings within experimentally determined ranges for monolayers (12.1−12.6 Å[90−94]) and bilayers (14.9−15.7

Å[90−95]) of interlayer water, respectively. The bulk water radial distribution was within 0.2 Å of the experimental distribution,[96] but calculated hydration energies were low (e.g., 7 kcal/mol for a monolayer of water sorbed to Ca-beidellite versus experimental observations of 12−15 kcal/mol[94,97]) and the density of the bulk was too high (1.1 g/cm^3). We find that all of the relevant observables can be adjusted over a wide range of values by small changes in the van der Waals and electrostatic parameters. Results of these ongoing parameter refinements will be described elsewhere.

Summary

In this paper, the first valence force field for molecular dynamics studies of clay minerals is reported. A new octahedral angle-bending potential was created through judicious choice of parameters for an existing quartic potential function. This insight allowed adaptation of many other parameters from the force field that Hill and Sauer[29] developed for tetrahedral aluminosilicates. All nonbonded potentials were revised so that larger atomic partial charges (which are in better agreement with MP2 calculations of related compounds and electron densities derived from X-ray crystallography) could be used, which in turn are expected to enable higher-quality modeling of clay interactions with charged and polar species.

The new force field parameters were fit to the crystal structures of quartz, gibbsite, kaolinite, and pyrophyllite, and successfully reproduced these structures with the exception of one hydroxyl orientation on kaolinite. New nonbonded parameters for Na^+ and Ca^{2+} were derived independently, based on the work of Åqvist.[71] Adsorbate parameters for these metals and for $HDTMA^+$ were successfully combined with the clay force field to model homoionic beidellites.

Acknowledgment. The authors thank two referees for extensive constructive criticism and Cliff Johnston for helpful comments. B.J.T. and P.M.B. were supported by financial assistance award DE-FC09-96SR18546 between the University of Georgia and the U.S. Department of Energy. D.M.M. and L.S. acknowledge partial support of this research through U.S. Department of Agriculture National Research Initiative Grant 95-37107-1915.

References and Notes

(1) Collins, D. R.; Catlow, C. R. A. *Mol. Simul.* **1990**, *4*, 341−346.
(2) Collins, D. R.; Catlow, C. R. A. *Am. Mineral.* **1992**, *77*, 1172−1181.
(3) Collins, D. R.; Stirling, W. G.; Catlow, C. R. A.; Rowbotham, G. *Phys. Chem. Miner.* **1993**, *19*, 520−527.
(4) Breu, J.; Catlow, C. R. A. *Inorg. Chem.* **1995**, *34*, 4504−4510.
(5) Delville, A. *Langmuir* **1991**, *7*, 547−555.
(6) Delville, A. *Langmuir* **1992**, *8*, 1796−1805.
(7) Delville, A. *J. Phys. Chem.* **1993**, *97*, 9703−9712.
(8) Delville, A.; Sokolowski, S. *J. Phys. Chem.* **1993**, *97*, 6261−6271.
(9) Skipper, N. T.; Refson, K.; McConnell, J. D. C. *J. Chem. Phys.* **1991**, *94*, 7434−7445.
(10) Skipper, N. T.; Chang, F.-R. C.; Sposito, G. *Clays Clay Miner.* **1995**, *43*, 285−293.
(11) Skipper, N. T.; Sposito, G.; Chang, F.-R. C. *Clays Clay Miner.* **1995**, *43*, 294−303.
(12) Chang, F.-R. C.; Skipper, N. T.; Sposito, G. *Langmuir* **1995**, *11*, 2734−2741.
(13) Boek, E. S.; Coveney, P. V.; Skipper, N. T. *Langmuir* **1995**, *11*, 4629−4631.
(14) Sato, H.; Yamagishi, A.; Kato, S. *J. Phys. Chem.* **1992**, *96*, 9377−9382.
(15) Sato, H.; Yamagishi, A.; Kato, S. *J. Phys. Chem.* **1992**, *96*, 9382−9387.
(16) Sato, H.; Yamagishi, A.; Nata, K.; Kato, S. *J. Phys. Chem.* **1996**, *100*, 1711−1717.
(17) Keldsen, G. L.; Nicholas, J. B.; Carrado, K. A.; Winans, R. E. *J. Phys. Chem.* **1994**, *98*, 279−284.
(18) Karaborni, S.; Smit, B.; Heidug, W.; Urai, J.; van Oort, E. *Science* **1996**, *271*, 1102−1104.
(19) Kawano, M.; Vessal, B.; Catlow, C. R. A. *J. Chem. Soc., Chem. Commun.* **1992**, 879−880.
(20) Bandyopadhyay, S.; Yashonath, S. *J. Phys. Chem.* **1995**, *99*, 4286−4292.
(21) Vayssilov, G. N. *Adv. Colloid Interface Sci.* **1993**, *43*, 51−85.
(22) Landis, C. R.; Root, D. M.; Cleveland, T. *Rev. Comput. Chem.* **1995**, *6*, 73−148.
(23) Allured, V. S.; Kelly, C. M.; Landis, C. R. *J. Am. Chem. Soc.* **1991**, *113*, 1−12.
(24) Rappé, A. K.; Casewit, C. J.; Colwell, K. S.; Goddard, W. A., III; Skiff, W. M. *J. Am. Chem. Soc.* **1992**, *114*, 10024−10035.
(25) Engelsen, S. B. Molecular Mechanics: Method Development and Application to Lipids. Ph.D. Dissertation, Technical University of Denmark, 1991.
(26) *MSI. Insight II User Guide*, Version 3.0.0; Molecular Simulations, Inc.: San Diego, CA, 1995.
(27) *MSI. Discover User Guide, Versions 2.9.5, 94.0, and 3.0.0*; Molecular Simulations, Inc.: San Diego, CA, 1995.
(28) Hill, J.-R.; Sauer, J. *J. Phys. Chem.* **1994**, *98*, 1238−1244.
(29) Hill, J.-R.; Sauer, J. *J. Phys. Chem.* **1995**, *99*, 9536−9550.
(30) Gibbs, G. V.; Downs, J. W.; Boisen, M. B., Jr. *Rev. Mineral.* **1994**, *29*, 331−368.
(31) Iishi, K. *Phys. Chem. Miner.* **1978**, *3*, 1−10.
(32) Hill, R. J. *Phys. Chem. Miner.* **1979**, *5*, 179−200.
(33) Sanders, M. J.; Leslie, M.; Catlow, C. R. A. *J. Chem. Soc., Chem. Commun.* **1984**, 1271−1273.
(34) Schröder, K.-P.; Sauer, J. *J. Phys. Chem.* **1996**, *100*, 11043−11049.
(35) Maple, J. R.; Hwang, M.-J.; Stockfish, T. P.; Dinur, U.; Waldman, M.; Ewig, C. S.; Hagler, A. T. *J. Comput. Chem.* **1994**, *15*, 162−182.
(36) Gibbs, G. V.; Hamil, M. M.; Louisnathan, S. J.; Bartell, L. S.; Yow, H. *Am. Mineral.* **1972**, *57*, 1578−1613.
(37) Gibbs, G. V.; Meagher, E. P.; Newton, M. D.; Swanson, D. K. In *Structure and Bonding in Crystals*; O'Keeffe, M., Navrotsky, A., Eds.; Academic Press, Inc.: New York, 1981; Vol. I, pp 195−225.
(38) Hill, R. J.; Gibbs, G. V. *Acta Crystallogr.* **1979**, *B35*, 25−30.
(39) Saalfeld, H.; Wedde, M. *Z. Kristallogr.* **1974**, *139*, 129−135.
(40) Lee, J. H.; Guggenheim, S. *Am. Mineral.* **1981**, *66*, 350−357.
(41) Bish, D. L. *Clays Clay Miner.* **1993**, *41*, 738−744.
(42) Szabo, A.; Ostlund, N. S. *Modern Quantum Chemistry: Introduction to Advanced Electronic Structure Theory*; Macmillan Publishing: New York, 1982.
(43) Levine, I. N. *Quantum Chemistry*, 4th ed.; Prentice Hall, Inc.: Englewood Cliffs, NJ, 1991.
(44) Krishnan, R.; Binkley, J. S.; Seeger, R.; Pople, J. A. *J. Chem. Phys.* **1980**, *72*, 650−654.
(45) McLean, A. D.; Chandler, G. S. *J. Chem. Phys.* **1980**, *72*, 5639−5648.
(46) Francl, M. M.; Pietro, W. J.; Hehre, W. J.; Binkley, J. S.; Gordon, M. S.; DeFrees, D. J.; Pople, J. A. *J. Chem. Phys.* **1982**, *77*, 3654−3665.
(47) Wong, M. W.; Gill, P. M. W.; Nobes, R. H.; Radom, L. *J. Phys. Chem.* **1988**, *92*, 4875−4880.
(48) Pulay, P.; Fogarasi, G.; Pongor, G.; Boggs, J. E.; Vargha, A. *J. Am. Chem. Soc.* **1983**, *105*, 7037−7047.
(49) Pople, J. A.; Schlegel, H. B.; Krishnan, R.; Defrees, D. J.; Binkley, J. S.; Frisch, M. J.; Whiteside, R. A.; Hout, R. F.; Hehre, W. J. *Int. J. Quantum Chem., Quantum Chem. Symp.* **1981**, *15*, 269−278.
(50) Frey, R. F.; Coffin, J.; Newton, S. Q.; Ramek, M.; Cheng, V. K. W.; Momany, F. A.; Schäfer, L. *J. Am. Chem. Soc.* **1992**, *114*, 5369−5377.
(51) Momany, F. A.; Rone, R.; Frey, R. F.; Schäfer, L. *Chemical Design Automation News* **1992**, *7*, 1,38−41.
(52) Chirlian, L. E.; Francl, M. M. *J. Comput. Chem.* **1987**, *8*, 894−905.
(53) Breneman, C. M.; Wiberg, K. B. *J. Comput. Chem.* **1990**, *11*, 361−373.
(54) Francl, M. M.; Carey, C.; Chirlian, L. E.; Gange, D. M. *J. Comput. Chem.* **1996**, *17*, 367−383.
(55) Teppen, B. J.; Miller, D. M.; Newton, S. Q.; Schäfer, L. *J. Phys. Chem.* **1994**, *98*, 12545−12557.
(56) Tsirelson, V. G.; Evdokimova, O. A.; Belokoneva, E. L.; Urusov, V. S. *Phys. Chem. Miner.* **1990**, *17*, 275−292.
(57) Downs, J. W.; Swope, R. J. *J. Phys. Chem.* **1992**, *96*, 4834−4840.
(58) Pauling, L. *Am. Mineral.* **1980**, *65*, 321−323.
(59) Lau, K. F.; Alper, H. E.; Thacher, T. S.; Stouch, T. R. *J. Phys. Chem.* **1994**, *98*, 8785−8792.
(60) Zhu, S.-B.; Singh, S.; Robinson, G. W. *Adv. Chem. Phys.* **1994**, *85* (Part 3), 627−731.
(61) Sposito, G. *The Surface Chemistry of Soils*; Oxford University Press, Inc.: New York, 1984.
(62) Lewis, J.; Schwarzenbach, D.; Flack, H. D. *Acta Crystallogr.* **1982**, *A38*, 733−739.
(63) Sasaki, S.; Fujino, K.; Takéuchi, Y.; Sadanaga, R. *Acta Crystallogr.* **1980**, *A36*, 904−915.

(64) Downs, J. W.; Hill, R. J.; Newton, M. D.; Tossell, J. A.; Gibbs, G. V. In *Electron Distribution and the Chemical Bond*; Coppens, P., Hall, M., Eds.; Plenum Press: New York, 1982; pp 178−190.
(65) Young, R. A.; Hewat, A. W. *Clays Clay Miner.* **1988**, *36*, 225−232.
(66) Levien, L.; Prewitt, C. T.; Weidner, D. J. *Am. Mineral.* **1980**, *65*, 920−930.
(67) Lager, G. A.; Jorgensen, J. D.; Rotella, F. J. *J. Appl. Phys.* **1982**, *53*, 6751−6756.
(68) Goldschmidt, V. M. *Naturwissenschaften* **1926**, *14*, 477−485.
(69) Pauling, L. *J. Am. Chem. Soc.* **1927**, *49*, 765−790.
(70) Whittaker, E. J. W.; Muntus, R. *Geochim. Cosmochim. Acta* **1970**, *34*, 945−956.
(71) Åqvist, J. *J. Phys. Chem.* **1990**, *94*, 8021−8024.
(72) Allen, M. P.; Tildesley, D. J. *Computer simulation of liquids*; Oxford University Press: Oxford, U.K., 1987.
(73) McQuarrie, D. A. *Statistical Thermodynamics*; Harper's Chemistry Series; Harper & Row Publishers, Inc.: New York, 1973.
(74) Karasawa, N.; Goddard, W. A., III. *J. Phys. Chem.* **1989**, *93*, 7320−7327.
(75) Giese, R. F.; Datta, P. *Am. Mineral.* **1973**, *58*, 471−479.
(76) Suquet, H.; Pezerat, H. *Clays Clay Miner.* **1987**, *35*, 353−362.
(77) de la Calle, C.; Suquet, H. *Rev. Mineral.* **1988**, *19*, 455−496.
(78) Cases, J. M.; Bérend, I.; Besson, G.; François, M.; Uriot, J. P.; Thomas, F.; Poirer, J. E. *Langmuir* **1992**, *8*, 2730−2739.
(79) Sato, T.; Watanabe, T.; Otsuka, R. *Clays Clay Miner.* **1992**, *40*, 103−113.
(80) Huang, W.-L.; Bassett, W. A.; Wu, T.-C. *Am. Mineral.* **1994**, *79*, 683−691.
(81) Kawano, M.; Tomita, K. *Clays Clay Miner.* **1991**, *39*, 77−83.
(82) Glaeser, R.; Méring, J. *C. R. Seances Acad. Sci., Ser. D* **1968**, *267*, 463−466.
(83) Lagaly, G. In *Layer Charge Characteristics of 2:1 Silicate Clay Minerals*; Mermut, A. R., Ed.; The Clay Minerals Society: Boulder, CO, 1994; pp 1−46.
(84) Malla, P. B.; Douglas, L. A. In *Proceedings of the International Clay Conference, Denver, 1985*; Schultz, L. G., van Olphen, H., Mumpton, F. A., Eds.; The Clay Minerals Society: Boulder, CO, 1987; pp 277−283.
(85) Boyd, S. A.; Mortland, M. M.; Chiou, C. T. *Soil Sci. Soc. Am. J.* **1988**, *52*, 652−657.
(86) Jaynes, W. F.; Boyd, S. A. *Soil Sci. Soc. Am. J.* **1991**, *55*, 43−48.
(87) Boyd, S. A.; Jaynes, W. F. In *Layer Charge Characteristics of 2:1 Silicate Clay Minerals*; Mermut, A. R., Ed.; The Clay Minerals Society: Boulder, CO, 1994; pp 47−77.
(88) Laird, D. A. In *Layer Charge Characteristics of 2:1 Silicate Clay Minerals*; Mermut, A. R., Ed.; The Clay Minerals Society: Boulder, CO, 1994; pp 79−103.
(89) Jaynes, W. F.; Traina, S. J.; Bigham, J. M.; Johnston, C. T. *Clays Clay Miner.* **1992**, *40*, 397−404.
(90) Mering, J. *Trans. Faraday Soc.* **1946**, *42B*, 205−219.
(91) Mooney, R. W.; Keenan, A. G.; Wood, L. A. *J. Am. Chem. Soc.* **1952**, *74*, 1371−1374.
(92) Glaeser, R.; Méring, J. *C. R. Seances Acad. Sci., Ser. D* **1968**, *267*, 463−466.
(93) Suquet, H.; de la Calle, C.; Pezerat, H. *Clays Clay Miner.* **1975**, *23*, 1−9.
(94) Fu, M. H.; Zhang, Z. Z.; Low, P. F. *Clays Clay Miner.* **1990**, *38*, 485−492.
(95) Slade, P. G.; Stone, P. A.; Radoslovich, E. W. *Clays Clay Miner.* **1985**, *33*, 51−61.
(96) Soper, A. K.; Phillips, M. G. *Chem. Phys.* **1986**, *107*, 47−60.
(97) Keren, R.; Shainberg, I. *Clays Clay Miner.* **1980**, *28*, 204−210.